

Finite Element Analysis of MHD Free Convection within Trapezoidal Enclosures with Uniformly Heated Side Walls

M. S. Hossain^{1*}, Mohammed Nasir Uddin², M. A. Alim³, M. Shobahani⁴

¹Department of Arts and Sciences, Ahsanullah University of Science & Technology (AUST), Dhaka-1208, Bangladesh

²Department of Mathematics, Bangladesh University of Business & Technology (BUBT), Dhaka, Bangladesh

³Department of Mathematics, Bangladesh University of Engineering & Technology (BUET), Dhaka-1000, Bangladesh

⁴Department of Mathematics and Natural Sciences, Brac University, Dhaka-1212, Bangladesh

Abstract: A numerical study is presented of two-dimensional laminar steady-state on magneto-hydrodynamics (MHD) free convection for heat flow patterns within trapezoidal enclosures. A finite element analysis is performed to investigate the effects of uniform heating and is also used for solving the Navier-Stokes and Energy balance equations. In this study, cold bottom walls, uniformly heated left and right (side) walls and insulated top walls with inclination angles (ϕ) are considered in a trapezoidal enclosure. The present numerical procedure adopted in this investigation yields consistent performance over a wide range of parameters, Prandtl numbers, ($Pr = 0.026 - 0.7$), and Rayleigh numbers ($Ra = 10^3 - 10^5$), Hartmann number ($Ha = 50$) with various tilt angles $\Phi = 45^\circ, 30^\circ$ and 0° (square). Numerical results are presented in terms of streamlines, isotherms, heat function (total heat flux) and nusselt numbers for different Ra and Pr . As Ra increases conduction dominant region changes for different Pr . Complete heat transfer analysis is performed in terms of local and average nusselt numbers.

Keywords: Free convection, Finite element method, Trapezoidal Enclosures, Uniform heating.

Nomenclature

B_0	Magnetic Induction
C_p	Specific Heat At Constant Pressure (J/Kg K)
G	Gravitational Acceleration (M/S^2)
Gr	Grashof Number
H	Convective Heat Transfer Coefficient ($W/M^2 K$)
Ha	Hartmann Number
K	Thermal Conductivity Of Fluid ($W/M K$)
L	Height Or Base Of Trapezoidal Cavity (M)
K	Thermal Conductivity Ratio Fluid
N	Total Number Of Nodes
Nu_{av}	Average Nusselt Number
Nu_{local}	Local Nusselt Number
P	Non-Dimensional Pressure
P	Pressure
Pr	Prandtl Number
Ra	Rayleigh Number
T	Non-Dimensional Temperature
T_h	Temperature Of Hot Bottom Wall (K)
T_c	Temperature Of Cold Bottom Wall (K)
U	X Component Of Dimensionless Velocity
U	X Component Of Velocity (M/S)
V	Y Component Of Dimensionless Velocity

V	Y Component Of Velocity (M/S)
V_0	Lid Velocity
X, Y	Cartesian Coordinates
X, Y	Dimensionless Cartesian Coordinates

Greek Symbols

α	Thermal Diffusivity (M^2/S)
β	Coefficient Of Thermal Expansion (K^{-1})
ρ	Density Of The Fluid (Kg/M^3)
$\Delta\theta$	Temperature Difference
θ	Fluid Temperature
M	Dynamic Viscosity Of The Fluid (Pa S)
Π	Heatfunction
N	Kinematic Viscosity Of The Fluid (M^2/S)
Σ	Fluid Electrical Conductivity ($\Omega^{-1}m^{-1}$)

Subscripts

B	Bottom Wall
L	Left Wall
R	Right Wall
S	Side Wall

I. Introduction

The well-known buoyancy driven Phenomena of convection motion of fluid has attracted many researchers over the past few years. The phenomenon of heat and mass transfer frequently exist in chemically processed industries such as food processing and polymer production. The phenomenon of free convection flow involving coupled heat and mass transfer occurs frequently in nature. In these studies the magnetohydrodynamic phenomenon is applied. Magnetohydrodynamics (MHD) has attracted the attention of a large number of scholars due to its diversified applications. The study of the effects of magnetic field on free convection flow is important in liquid-metals, electrolytes and ionized gases. Magnetohydrodynamic flows have applications in meteorology, solar physics, cosmic fluid dynamics, astrophysics, geophysics and in the motion of earth's core. Shanker and Kishan [1] presented the effect of mass transfer on the MHD flow past an impulsively started infinite vertical plate. Elabashbeshy [2] studied heat and mass transfer along a vertical plate in the presence of magnetic field. However, Free convection in enclosed cavities has received significant attention due to many engineering applications [3–7]. The extensive studies for rectangular and square enclosures using various numerical simulations reported by Patterson and Imberger [8], Nicolette et al.[9], Hall et al. [10], Hyun and Lee [11], Fusegi et al. [12], Lage and Bejan [13,14], Xia and Murthy [15] and Al-Amiri et al.[16] ensure that several attempts have been made to acquire a basic understanding of natural convection flows and heat transfer characteristics in an enclosure. The majority of works dealing with convection in enclosures are restricted to the cases of simple geometry e.g., rectangular, square, cylindrical and spherical cavities. But the configurations of actual containers occurring in practice are often far from being simple. A few studies on natural convection on triangular enclosures filled with a viscous fluid or a porous medium have been carried out by earlier researchers [17–19]. In recent years, most of the enclosures commonly used in industries are cylindrical, rectangular, trapezoidal, triangular etc. Trapezoidal enclosures have also received a considerable attention for their application in various fields.

A comprehensive understanding of energy flow and entropy generation is needed for an optimal process design via reducing irreversibilities in terms of ‘entropy generation’. In this study, analysis on entropy generation during natural convection in a trapezoidal cavity with various inclination angles ($\phi = 45^\circ, 60^\circ$ and 90°) have been carried out for an efficient thermal processing of various fluids of industrial importance ($Pr = 0.015, 0.7$ and 1000) in the range of Rayleigh number ($10^3 - 10^5$) by Basak et. al [20]. Basak et al. [21] studied a comprehensive heatline based approach for natural convection flows in trapezoidal enclosures with the effect of various walls heating. The present numerical study deals with natural convection flow in closed trapezoidal enclosures. Anandalakshmi and Basak [22] studied for the energy distribution and thermal mixing in steady laminar natural convective flow through the rhombic enclosures with various inclination angles, ϕ for various industrial applications. Here simulations are carried out for various regimes of Prandtl (Pr) and Rayleigh (Ra) numbers. Dimensionless streamfunctions and heatfunctions are used to visualize the flow and energy distribution, respectively. Basak et al. [23] also investigated the numerical investigation of natural convection in a porous trapezoidal enclosures for uniformly or non-uniformly heated bottom wall. Penalty finite element analysis with bi-quadratic elements is used for solving the Navier–Stokes and energy balance equations. The numerical solutions are studied in terms of streamlines, isotherms, heatlines, local and average Nusselt numbers for a wide range of parameters $Da(10^{-5}-10^{-3})$, $Pr(0.015-1000)$ and $Ra(Ra = 10^3-10^6)$. At low Darcy number ($Da = 10^{-5}$), heat transfer is primarily due to conduction for all ϕ 's as seen from the heatlines which are normal to the isotherms. Basak et al. [24] also performed heat flow patterns in the presence of natural convection within trapezoidal enclosures with heatlines concept. In this study, natural convection within a trapezoidal enclosure for uniformly and non-uniformly heated bottom wall, insulated top wall and isothermal side walls with inclination angle have been investigated. Momentum and energy transfer are characterized by streamfunctions and heatfunctions, respectively, such that streamfunctions and heatfunctions satisfy the dimensionless forms of momentum and energy balance equations, respectively. Finite element method has been used to solve the velocity and thermal fields and the method has also been found robust to obtain the streamfunction and heatfunction accurately. The unique solution of heatfunctions for situations in differential heating is a strong function of Dirichlet boundary condition which has been obtained from average Nusselt numbers for hot or cold regimes. Natarajan et. al [25] presented a numerical study of combined natural convection and surface radiation heat transfer in a solar trapezoidal cavity absorber for Compact Linear Fresnel Reflector (CLFR) . The numerical simulation results are presented in terms of Nusselt number correlation to show the effect of these parameters on combined natural convection and surface radiation heat loss.

In the present investigation, visualization of heat flows via heatlines for magneto-hydrodynamics (MHD) free convection with uniformly heated side walls were reported for trapezoidal enclosures. Results are obtained to display the circulations and for different physical parameters in terms of streamlines, stream functions, total heat flux, isotherms and heat transfer rates for the walls in terms of average and local nusselt numbers.

II. Model Specification

The geometry for the configuration with the system of co-ordinates is schematically shown in Fig. 1. The model considered here is a two-dimensional trapezoidal enclosures of height L with the left wall inclined at an angle $\phi = 45^\circ, 30^\circ, 0^\circ$ with Y axis. Here left wall and right (side) walls are subjected to hot T_h temperature; bottom wall is subjected to cold T_c temperature while the top wall is kept insulated. The boundary conditions for velocity are considered as no-slip on solid boundaries.

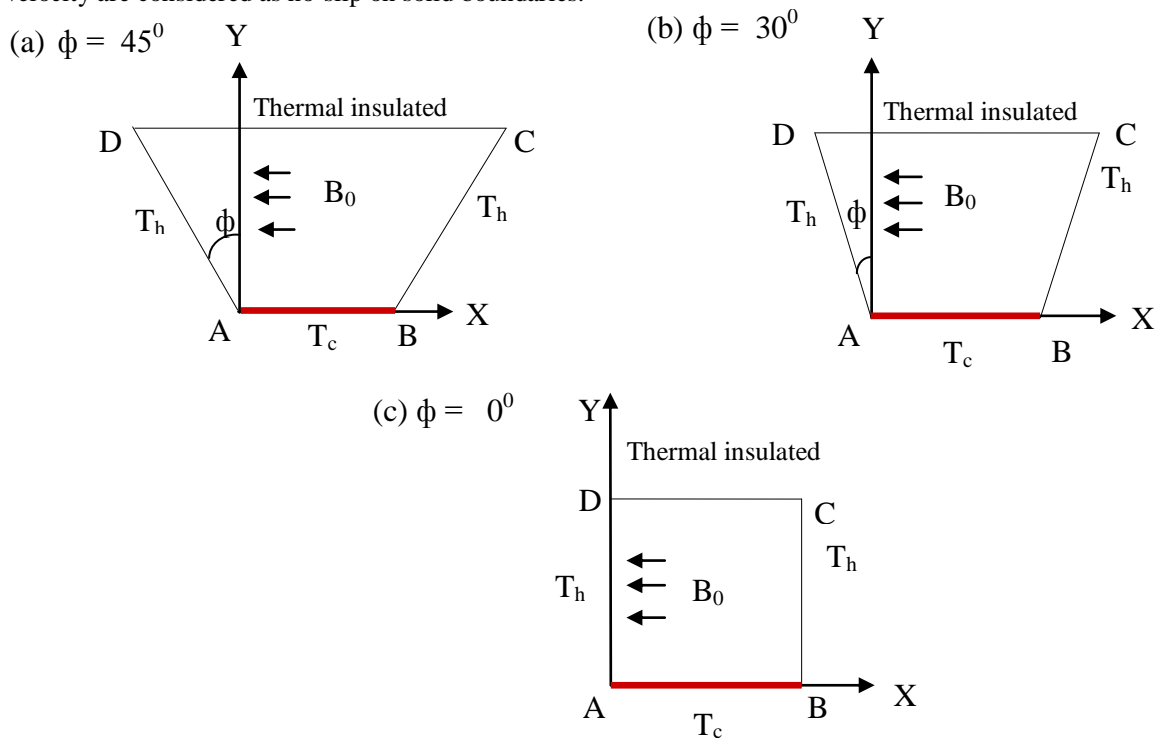


Figure 1: Schematic diagram of the physical system for (a) $\phi = 45^\circ$ (b) $\phi = 30^\circ$ and (c) $\phi = 0^\circ$

2.1 Mathematical Formulation

The flow inside the cavity is assumed to be two-dimensional, steady, laminar and incompressible and the fluid properties are said to be constant. For the treatment of buoyancy term in the momentum equation, Boussinesq approximation is used. The dimensionless governing equations describing the flow are as follows:

Continuity Equation

$$\frac{\partial U}{\partial X} + \frac{\partial V}{\partial Y} = 0 \quad (1)$$

Momentum Equations

$$U \frac{\partial U}{\partial X} + V \frac{\partial U}{\partial Y} = -\frac{\partial P}{\partial X} + \text{Pr} \left(\frac{\partial^2 U}{\partial X^2} + \frac{\partial^2 U}{\partial Y^2} \right) \quad (2)$$

$$U \frac{\partial V}{\partial X} + V \frac{\partial V}{\partial Y} = -\frac{\partial P}{\partial Y} + \text{Pr} \left(\frac{\partial^2 V}{\partial X^2} + \frac{\partial^2 V}{\partial Y^2} \right) + Ra \text{Pr} \theta - Ha^2 \text{Pr} V \quad (3)$$

Energy Equation

$$U \frac{\partial \theta}{\partial X} + V \frac{\partial \theta}{\partial Y} = \left(\frac{\partial^2 \theta}{\partial X^2} + \frac{\partial^2 \theta}{\partial Y^2} \right) \quad (4)$$

The Following definitions and dimensionless parameters are used in writing equations (1-4) as,

$$X = \frac{x}{L}, \quad Y = \frac{y}{L}, \quad U = \frac{uL}{\alpha}, \quad V = \frac{vL}{\alpha}, \quad P = \frac{pL^2}{\rho\alpha^2}, \quad \theta = \frac{T - T_c}{T_h - T_c}, \quad \text{Pr} = \frac{\nu}{\alpha},$$

$$Gr = \frac{g\beta L^3 (T_h - T_c)}{\nu^2}, \quad Ra = \frac{g\beta L^3 (T_h - T_c) \text{Pr}}{\nu^2}, \quad Ha^2 = \frac{\sigma B_0^2 L^2}{\mu}, \quad \alpha = \frac{k}{\rho C_p}$$

Here Ha , Ra , Pr , Gr are Hartmann number, Rayleigh number, Prandtl number and Grashof number respectively. Thermal diffusivity, volumetric thermal expansion coefficient, dynamic viscosity, kinematic viscosity, electrical conductivity, density and dimensional temperature difference of the fluid are represented by the symbols α , β , μ , ν , σ , ρ , ΔT , respectively.

2.2 Boundary Conditions

The boundary conditions (also shown in Fig. 1), for the present problem are specified as follows:

At the bottom wall:

$$U = 0, V = 0, \theta = 1, \quad \forall Y = 0, \quad 0 \leq X \leq 1$$

At the left wall:

$$U = 0, V = 0, \theta = 0, \quad \forall X \cos \phi + Y \sin \phi = 0, \quad 0 \leq Y \leq 1$$

At the right wall:

$$U = 0, V = 0, \theta = 0, \quad \forall X \cos \phi - Y \sin \phi = \cos \phi, \quad 0 \leq Y \leq 1$$

At the top wall:

$$U = 0, V = 0, \frac{\partial \theta}{\partial Y} = 0, \quad \forall Y = 1, \quad -\tan \phi \leq X \leq (1 + \tan \phi)$$

where X and Y are dimensionless coordinates varying along horizontal and vertical directions, respectively; U and V are dimensionless velocity components in X and Y directions, respectively; θ is the dimensionless temperature.

The local Nusselt number at the heated surface of the cavity which is defined by the following expression:

$$Nu_l = Nu_r = Nu_b = Nu_s = -\frac{\partial \theta}{\partial n}$$

where n denotes the normal direction on a plane.

The average Nusselt number at the cold bottom wall, uniformly heated left and right (side) walls and insulated top walls of the enclosures based on the non-dimensional variables may be expressed as,

$$Nu = \int_0^1 Nu_l dX = \int_0^1 Nu_r dX = \int_0^1 Nu_s dX = \int_0^1 Nu_b dX$$

The non-dimensional stream function is defined as, $U = \frac{\partial \Psi}{\partial Y}$, $V = -\frac{\partial \Psi}{\partial X}$

III. Research Methodology

Finite element analysis is a method to solve differential equations numerically which can be applied to many problems in engineering and scientific fields. Finite element simulation of free convection in a two-dimensional trapezoidal enclosures has been studied. This research starts from two-dimensional Navier-Stokes equations together with the energy equation to obtain the corresponding finite element equations. Galerkin's weighted residual method is applied to discretize the non-dimensional governing equations. Triangular mesh is used to obtain the solution. Because this type of mesh can be used in any shape of domain. Details of method are available in Taylor and Hood [26] and Dechaumphai [27].

IV. Grid Independence Test

In order to determine the proper grid size for this study, a grid independence test are conducted with $Pr = 0.7$, $\phi = 45^\circ$, $Ha = 50$ and $Ra = 10^5$. The following five types of mesh are considered for the grid independence test. These grid densities are 1527, 2541, 3573, 4563, 5858 nodes and 216, 365, 527, 668, 864 elements. Average Nusselt numbers at the heated surface study of trapezoidal enclosures are used as a measure of accuracy of solution. From the table 1, a grid size of 4563 nodes and 668 elements is chosen for better accuracy.

Nodes	1527	2541	3573	4563	5858
(Elements)	(216)	(365)	(527)	(668)	(864)
Nu	1.751726	1.747969	1.834902	1.848767	2.050656
Time (s)	4.609	5.672	7.204	8.016	9.625

Table1: Grid Sensitivity Check at $Pr = 0.7$, $\phi = 45^\circ$, $Ha = 50$ and $Ra = 10^5$.

V. Code Validation

The present numerical solution is validated by comparing the current code results against the numerical result of Basak et al. [24] for free convection in a trapezoidal cavity for streamlines, isotherms and heatflux. For three different Rayleigh numbers ($Ra = 10^3, 10^4$ and 10^5), while the prandtl number and angle are fixed i.e. $Pr = 0.7, \phi = 45^\circ$ for uniform heating of side wall, average Nusselt number is calculated. The numerical solutions (present work and Basak et al. [24]) are in good agreement.

Ra	Average Nusselt Number, (Nu_{av})	
	Present work	Basak et al. (March 2009)
	$\phi = 45^\circ$	$\phi = 45^\circ$
10^3	1.672972	1.27778
10^4	1.842988	1.83453
10^5	2.797346	2.71105

Table 2: Code Validation For Uniform Heating of Side Wall With $Pr = 0.7$.

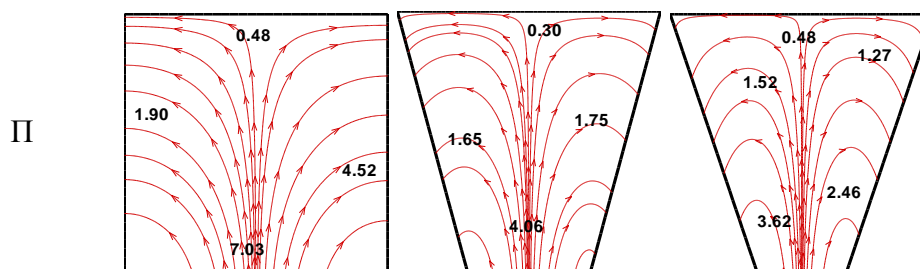
VI. Results And Discussion

In this section we present numerical results for streamlines, isotherms and heat function or heatflux for different Rayleigh number $Ra = 10^3 - 10^5$ and Prandtl number, $Pr = 0.026, 0.7$ for the fluid with various angles, $\phi = 45^\circ, 30^\circ, 0^\circ$. These are shown in figure (2-4). Addition, heat transfer rate for local and average nusselt numbers have been shown for various values of Rayleigh and Prandtl numbers and angles ϕ .

6.1 Uniform Heating

Figure 2 shows the effects of streamlines, isotherms and heat function for Rayleigh numbers. Here the magnitudes of streamfunction and heat transfers are primarily due to conduction at low Rayleigh number. Isotherms with $\theta = 0.10 - 0.20$ take place symmetrically along side (left or right) walls and with $\theta \geq 0.30$ are smooth curves symmetric with respect to vertical symmetrical line for $Ra = 10^3, Pr = 0.026$ and $\phi = 0^\circ$ (square cavity) (Fig. 2a). Again, for $Ra = 10^3, Pr = 0.026$ and $\phi = 30^\circ$ the temperature contours with $\theta = 0.10 - 0.40$ come about symmetrically near the side walls of the enclosure and with $\theta \geq 0.50$ are smooth curves symmetric with respect to central symmetrical line (Fig. 2b). Also for $Ra = 10^3, Pr = 0.026$ and $\phi = 45^\circ$ isotherms (temperature) with $\theta = 0.10 - 0.50$ arise symmetrically near the side walls of the enclosure and with $\theta \geq 0.60$ are smooth curves symmetric with respect to vertical symmetrical line (Fig. 2c). The heatlines or total heat flux or heat function are shown in panels of fig 2a-c. The heatlines illustrate similar attribute that were observed for uniform heating cases. Besides, we see that vortices are obtained for streamlines in fig 2a-c.

The interesting message is that at the bottom corner point $\phi = 0^\circ$ (square cavity) is superior to $\phi = 45^\circ$ and 30° . It is evident that heatlines near the bottom portion of side walls are more dense for $\phi = 45^\circ$ and less dense for $\phi = 0^\circ$ (square cavity). The dense heatlines are also indicating enhanced rate of heat transfer from the bottom to the side walls. Therefore for $\phi = 45^\circ$ isotherms with $\theta = 0.05 - 0.35$ are shifted toward the side walls. It is also observed that at the top portion of the cavity for $\phi = 45^\circ$ and 30° heat transfer is higher compressed to $\phi = 0^\circ$ (square cavity) based on value of heatfunction (Π). At the corners of bottom wall as the heat transfer is quite large, the thermal boundary layer is found to develop near the bottom edges and thickness of boundary layer is bigger at the top portion of the cold wall signifying less heat transfer to the top portion.



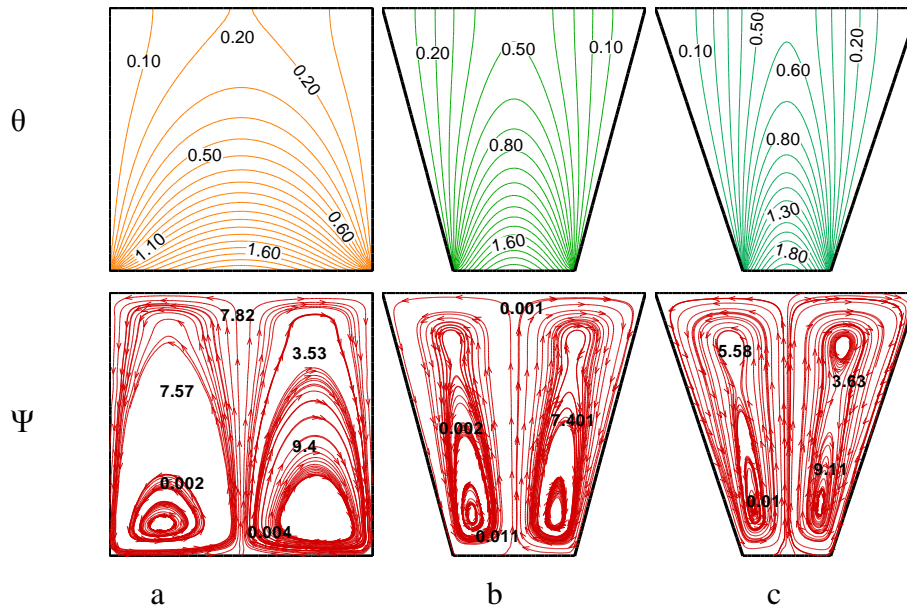
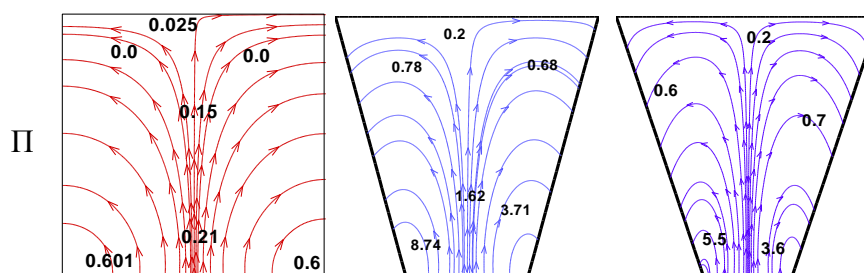


Figure 2: Stream function (Ψ), temperature (θ), heat function or total heat flux (Π) for uniform bottom heating $\theta(X,0) = 1$ with $Pr = 0.026$, $Ha = 50$ and $Ra = 10^3$ (a) $\Phi = 0^\circ$ (b) $\Phi = 30^\circ$ (c) $\Phi = 45^\circ$

Figure 3 shows that the magnitudes of streamfunction are smaller for $Ra = 10^5$, $Pr = 0.026$ and isotherms (temperature) with $\theta = 0.05 - 0.15$, $\theta = 0.05 - 0.30$, $\theta = 0.05 - 0.35$ occur symmetrically near the side walls of the enclosure and with $\theta \geq 0.25$, $\theta \geq 0.30$, $\theta \geq 0.35$ are smooth curves symmetric with respect to central symmetrical line for $Ra = 10^5$, $Pr = 0.026$ and $\phi = 45^\circ, 30^\circ, 0^\circ$ (square cavity) (Fig 5.9a-c, 5.10a-c) and heatlines enhanced the rate of heat transfer from the bottom to side walls for $Ra = 10^4$, $Pr = 0.026$. It is observed that at critical Ra the middle portion of isotherms starts getting deformed and the maximum value of ψ is at the eye of vortices. As Ra increases, the buoyancy driven circulation inside the cavity is also increased as seen from greater magnitudes of stream function (fig. 3). It is also observed that the greater circulation in bottom regime follows a progressive wrapping and isotherms are more compressed towards the side wall as can be seen figure 3.

Figure 4 demonstrates that the magnitudes of streamfunction are circular or elliptical near the core but the streamlines near the wall is almost parallel to wall exhibiting large intensity of flow for $Pr = 0.7$ and $Ra = 10^5$. Vortices are also enhanced for every case of enclosures. Also for $Pr = 0.7$ isotherms with $\theta = 0.05 - 0.15$, $\theta = 0.05 - 0.45$, $\theta = 0.05 - 0.50$ for 0.7 and $Ra = 10^5$ transpire symmetrically near the side walls of the enclosure and $\theta \geq 0.20$, $\theta \geq 0.50$, $\theta \geq 0.55$ are flat curves symmetric with respect to central symmetrical line for $Ra = 10^5$, $Pr = 0.7$ and $\phi = 45^\circ, 30^\circ, 0^\circ$ (square cavity). The detection is that for

irrespective of angles ϕ the intensity of flow has been increased as seen in fig 3. Although for intensity of flow streamlines near the wall is almost parallel to wall but streamlines look like circular or elliptical near the core (see figure 3). It is fascinating that multiple correlations are absent for $Pr = 0.7$ and $Ra = 10^5$. Due to enhanced flow circulations the isotherms are highly compressed near the side walls except near the bottom wall especially for $\phi = 45^\circ$ and 30° . The large temperature gradient near the side walls are due to noteworthy number of heatlines with a large variation of heatfunction as seen in figure 4a-c .



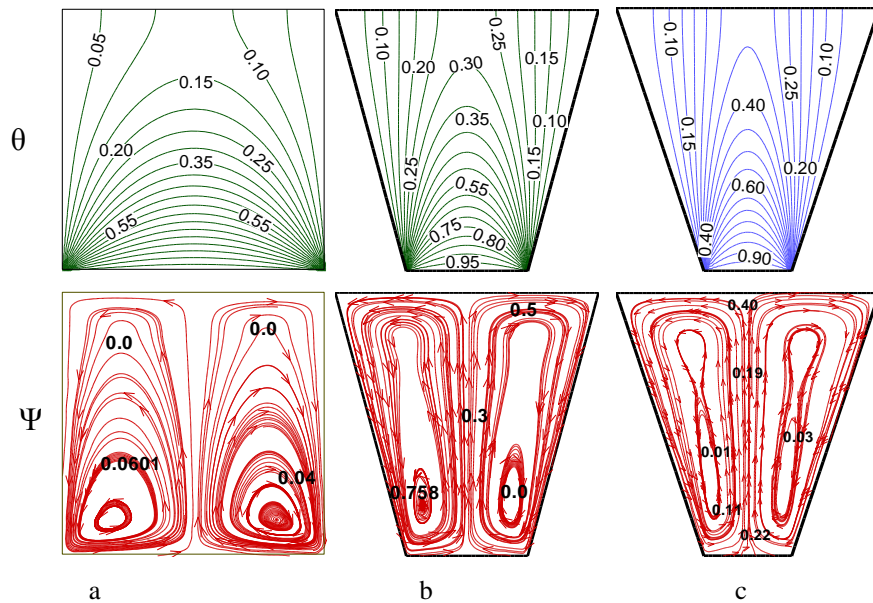


Figure 3: Stream function (Ψ), temperature (θ), heat function or total heat flux(Π) for uniform heating of side wall $\theta(X,0) = 1$ with $Pr = 0.026$, $Ha = 50$ and $Ra = 10^5$ (a) $\Phi = 0^\circ$ (b) $\Phi = 30^\circ$ (c) $\Phi = 45^\circ$

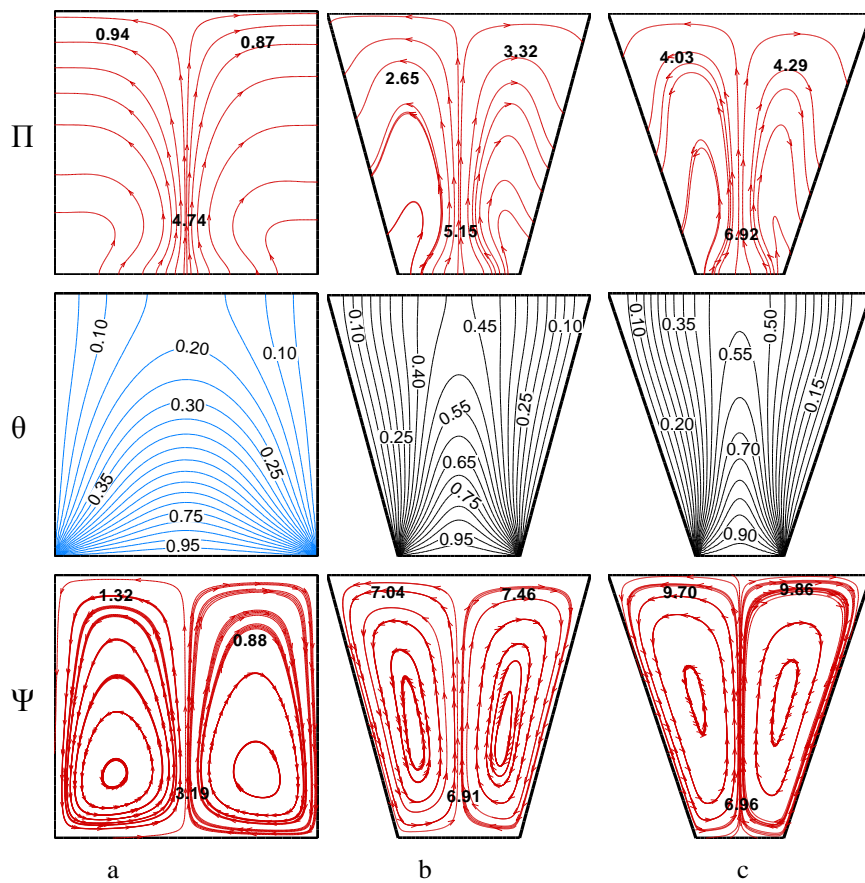


Figure 4: Stream function (Ψ), temperature (θ), heat function or total heat flux(Π) contours for uniform bottom heating $\theta(X,0) = 1$ with $Pr = 0.7$, $Ha = 50$ and $Ra = 10^5$ (a) $\Phi = 0^\circ$ (b) $\Phi = 30^\circ$ (c) $\Phi = 45^\circ$

6.2 Heat Transfer Rates: Local And Average Nusselt Numbers

Figure 5(a-c) shows the effect of local heat transfer rates (Nu_s) vs distance for various inclination tilt angles i.e. for $\phi = 0^\circ, 30^\circ, 45^\circ$ when $Ra = 10^3$ and $Pr = 0.7$ for uniform heating of side wall. It is observed that local heat transfer rate is maximum at the bottom edge of side wall and thereafter decreases sharply upto a point which is very near to the bottom edge. It is seen that Nu_s increase upto a point near to the top wall and also decreases with distance near to the bottom wall. The boundary layer starts to form at the bottom edge of the side wall and the boundary layer thickness is quite large near the bottom wall for all ϕ s. Due to large intensity of convection at $Ra = 10^3$ the thickness of the boundary layers are small at the middle portions of side walls and is found to be larger near the top portion. But also figure 5(b-c) shows the similar effects of local heat transfer rates (Nu_s) with distance for same Pr and different Ra respectively. As Ra increases, magnitudes of local heat transfer rates become smaller and maximum heat transfer occurs near the top portion. It may be mentioned that the larger degree of compression of isotherms for uniform heating case results in larger and $Nu_{s(local)}$ is quite large near to the bottom wall.

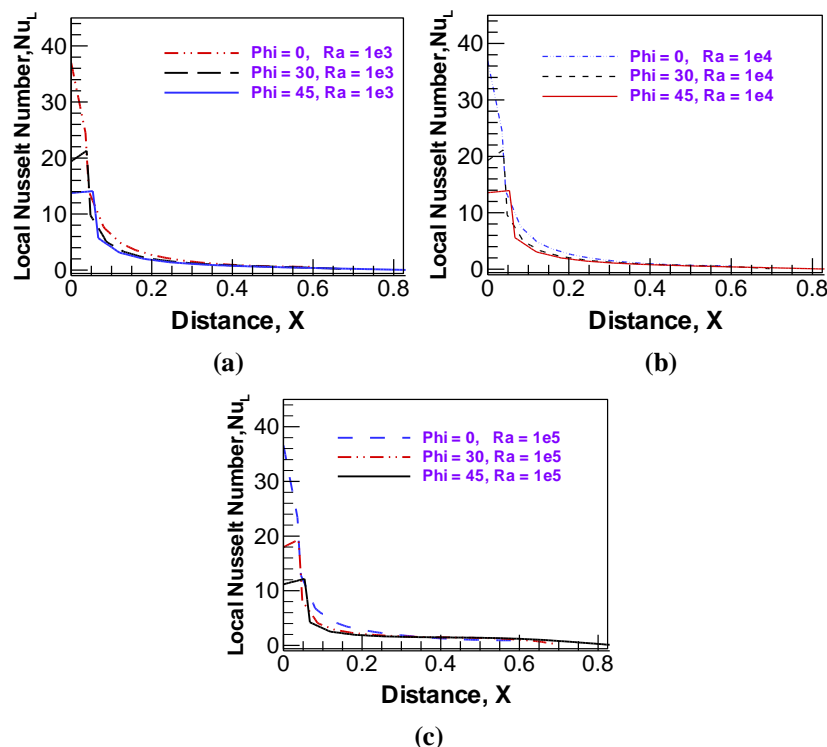


Figure 5: Variations of local Nusselt numbers (Nu_s) with distance for different Rayleigh numbers, (a) $Ra = 10^3$, (b) 10^4 , (c) 10^5 and angles $\Phi = 0^\circ, 30^\circ, 45^\circ$ when $Pr = 0.7$

The heat transfer rates are presented in figure 6(a)-(c), where distributions of average Nusselt number are plotted vs the logarithmic Rayleigh number respectively. Here figure 6(a)-(c) illustrates uniform heating of side walls respectively. It may be noted that average Nusselt number is obtained by considering temperature gradient. It also be noted that as Ra increases then the average Nusselt number increases. It is seen in figure 6(a) that as Ra increases from 10^3 - 10^5 then average Nusselt number is straightly moving for $\Phi = 0^\circ, 30^\circ$ but for $\Phi = 45^\circ$ Ra increases more when $Pr = 0.026$. As Pr increases (figure 6(b)) then conduction dominant heat transfer is narrowed down. It is also seen from figure 6(c) that, as Pr increases more than from uniform heating case it is analyzed that average Nusselt number for bottom wall is also slightly increasing during the entire Rayleigh number regime.. As Pr increases then for conduction dominant heat transfer, the average Nusselt number is generally constant irrespective of Ra . It is observed that Nu_s at the middle portion of bottom wall for $\Phi = 0^\circ$ is larger for uniform heating case whereas for $\Phi = 30^\circ$ and 45° heat transfer rates are identical. It is also observed that when $Pr = 0.026$, heat transfer rates for $\Phi = 45^\circ$ is swiftly increasing except $\Phi = 30^\circ$ and 0° .

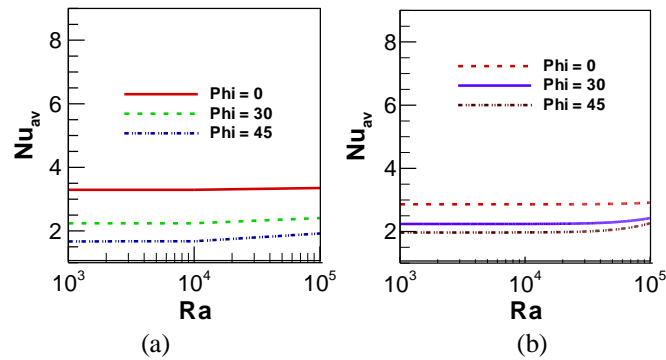


Figure 6: Variations of Average Nusselt Number vs Rayleigh number for (a) $Pr = 0.026$, (b) $Pr = 0.7$ and of angles $\Phi = 0^\circ, 30^\circ, 45^\circ$ for uniform heating of side wall.

VII. Conclusions

The problem of MHD free convection within trapezoidal enclosures for uniformly heated side wall with heatlines concept has been studied numerically. Flow and temperature field in terms of streamlines and isotherms and heat function or total heat flux have been displayed. The results of the numerical analysis lead to the following conclusions:

- Local Nusselt number of uniform heating of side wall is largest at the bottom edge of the side wall and thereafter that decreases sharply upto a point which is very near to the bottom edge.
- The heat transfer rate average Nusselt Number, Nu_{av} increases with the increase of Rayleigh number, Ra , for uniform heating of side wall.
- The maximum rate of heat transfer is obtained for the highest Pr .
- Various vortices entering into the flow field and secondary vortex at the vicinity boundary wall and bottom wall of the cavity is seen in the streamlines.
-

Acknowledgements

Authors would like to express their gratitude to the Department of Mathematics, Bangladesh University of Engineering and Technology (BUET) and Department of Arts and Sciences, Ahsanullah University of Science and Technology (AUST), Dhaka, Bangladesh, for providing computing facility during this work.

References

- [1] Lhl Shanker B. and Kishan N., The effects of mass transfer on the MHD flow past an impulsively started infinite vertical plate with variable temperature or constant heat flux, *J. Eng. Heat Mass Transfer*, 19, 1997, 273-278.
- [2] Elabashbeshy E.M.A. , Heat and mass transfer along a vertical plate with variable temperature and concentration in the presence of magnetic field, *Int. J. Eng. Sci.*, 34, 1997, 515-522. doi:10.1016/S0020-7225(96)00089-4
- [3] J.M. Garrpeters, The neutral stability of surface-tension driven cavity flows subject to buoyant forces 1. Transverse and longitudinal disturbances, *Chem. Eng. Sci.* 47 (5), 1992, 1247–1264.
- [4] L.B. Wang, N.I. Wakayama, Control of natural convection in non- and low-conducting diamagnetic fluids in a cubical enclosure using inhomogeneous magnetic fields with different directions, *Chem. Eng. Sci.* 57 (11), 2002, 1867–1876.
- [5] I.E. Sarris, I. Lekakis, N.S. Vlachos, Natural convection in a 2D enclosure with sinusoidal upper wall temperature, *Num Heat Transfer A* 42 (2002) 513–530.
- [6] A. Ousegui, A. Le Bail, M. Havet, Numerical and experimental study of a natural convection thawing process, *AIChE J.* 52 (12), 2006, 4240–4247.
- [7] O.G. Martynenko, P.P. Khramtsov, *Free-Convective Heat Transfer*, Springer, Berlin, 2005.
- [8] J. Patterson, J. Imberger, Unsteady natural convection in a rectangular cavity, *J.Fluid Mech.*, 100, 1980, 65–86.
- [9] V.F. Nicolette, K.T. Yang, J.R. Lloyd, Transient cooling by natural convection in atwo-dimensional square enclosure, *Int. J. Heat Mass Transfer*, 28 , 1985, 1721–1732.
- [10] J.D. Hall, A. Bejan, J.B. Chaddock, Transient natural convection in a rectangular enclosure with one heated side wall, *Int. J. Heat Fluid Flow*, 9, 1988, 396–404.
- [11] J.M. Hyun, J.W. Lee, Numerical solutions of transient natural convection in a square cavity with different sidewall temperature, *Int. J. Heat Fluid Flow*, 10, 1989, 146–151.
- [12] T. Fusegi, J.M. Hyun, K. Kuwahara, Natural convection in a differentially heated square cavity with internal heat generation, *Num. Heat Transfer A*, 21, 1992, 215–229.
- [13] J.L. Lage, A. Bejan, The Ra - Pr domain of laminar natural convection in an enclosure heated from the side, *Num. Heat Transfer A* , 19 , 1991, 21–41.
- [14] J.L. Lage, A. Bejan, The resonance of natural convection in an enclosure heated periodically from the side, *Int. J. Heat Mass Transfer*, 36, 1993, 2027–2038.
- [15] C. Xia, J.Y. Murthy, Buoyancy-driven flow transitions in deep cavities heated from below, *ASME Trans. J. Heat Transfer*, 124, 2002, 650–659.
- [16] A.M. Al-Amiri, K.M. Khanafer, Pop I, Numerical simulation of combined thermal and mass transport in a square lid-driven cavity, *Int. J. Thermal Sci.*, 46(7), 2007, 662–671.

- [17] Y.E. Karyakin, Y.A. Sokovishin, O.G. Martynenko, Transient natural convection in triangular enclosures, *Int. J. Heat Mass Transfer*, 31, 1988, 1759–1766.
- [18] A. Bejan, D. Poulikakos, Natural convection in an attic shaped space filled with porous material, *J. Heat Transfer – Trans. ASME*, 104, 1982, 241–247.
- [19] D. Poulikakos, A. Bejan, Numerical study of transient high Rayleigh number convection in an attic-shaped porous layer, *J. Heat Transfer – Trans. ASME*, 105, 1983, 476–484.
- [20] Bm, T. Basak, R. Anandalakshmi, Kumar Pushpendra, S. Roy, “Entropy generation vs energy flow due to natural convection in a trapezoidal cavity with isothermal and non-isothermal hot bottom wall”, *Energy*, 37, January 2012, 514.
- [21] T. Basak, D. Ramakrishna, S. Roy, A. Matta, I. Pop, “A comprehensive heatline based approach for natural convection flows in trapezoidal enclosures: Effect of various walls heating”, *International Journal of Thermal Sciences*, 50 (8), August 2011, 1385-1404.
- [22] R. Anandalakshmi, T. Basak, “Heat flow visualization for natural convection in rhombic enclosures due to isothermal and non-isothermal heating at the bottom wall”, *International Journal of Heat and Mass Transfer*, 55(4), 31 January 2012, 1325 - 1342.
- [23] Basak T., Roy S., Matta A. , Pop I., “Analysis of heatlines for natural convection within porous trapezoidal enclosures: Effect of uniform and non-uniform heating of bottom wall” *International Journal of Heat and Mass Transfer*, Vol. 53, Issues 25–26, pp. 5947-5961, December 2010.
- [24] T. Basak, S. Roy, and I. Pop, Heat flow analysis for natural convection within trapezoidal enclosures based on heatline concept, *Int.J. Heat Mass Transfer*, 52, March 2009, 2471-2483.
- [25] S. K. Natarajan, K.S. Reddy, and T. K. Mallick, “Heat loss characteristics of trapezoidal cavity receiver for solar linear concentrating system”, *Applied Energy*, 93, May 2012, 523-531.
- [26] C. Taylor and P. Hood, , “A Numerical Solution of the Navier-Stokes Equations Using Finite Element technique”, *1(Computer and Fluids 1)*, 73,1973. doi:10.1016/0045-7930(73)90027-3
- [27] P. Dechaumphai, *Finite Element Method in Engineering*, 2nd ed., Chulalongkorn University Press, Bangkok, 1999.